Chapter 5

Applications of Fiber Optic Displacement Sensor

5.1 Introduction

As discussed in earlier chapters, fiber-optic displacement sensors (FODS) have many advantages such as low cost, ease of installation and high sensitivity. This sensor facilitates optical multimode plastic bundled fiber as probe in conjunction with intensity modulation technique. The proposed FODSs are capable of providing a large sensing dynamic range, which in turn allows a more accurate displacement measurement. Beside displacement measurement, the FODS can also be used to sense many other parameters such as temperature, pressure, refractive index, strain, mass and etc [1-3]. In this chapter, applications of FODS such as detection of metal surface roughness, liquid refractive index, liquid level, as well as vibration will be discussed. In the detection of metal surface roughness, a light beam is launched onto the metal surface via a bundled fiber. The reflected light from the surface is collected by the bundled fiber and routed to a photodiode. The output voltage from the photodiode is measured as a function of distance between the bundled fiber output and metal surface to estimate the surface roughness. On the other hand, application of FODSs in liquid refractive index measurement is investigated theoretically and experimentally and a FODS is used for sensing of glucose concentration in distilled water.

Continuous monitoring of liquid level is also demonstrated using FODS. For vibration measurement, a simple sensor design is proposed using FODS with a bundled fiber probe.

5.2 The Estimation of Metal Surface Roughness

FODS offers the possible development of a variety of sensors for a wide range of applications [4]. One of the applications is to estimate the surface roughness of various materials. Quantitative estimation of surface roughness can be obtained by various mechanical and optical techniques [5]. The advantages of optical technique over their mechanical counterparts include their non-contact nature and in-situ measurement as well as rapid measurement capability [6-7]. Application of FODS as displacement sensor involves a transmitting fiber which incident a laser beam onto the target surface and multiple receiving fibers surrounding the transmitting fiber to collect the reflected light off the target surface. Displacement measurement is based on the comparison of reflected light intensity against that of the launch light. For surface roughness estimation, FODS is based on intensity modulation technique and the object is placed within the linear response range of the displacement curve.

Experimental set-up of the fiber optic sensor is shown in Fig. 5-1. It consists of a light source, chopper, concentric type bundled fiber and a silicon detector connected to a lock-in amplifier and a computer for signal analysis. The bundled fiber is 2m long

and consists of one transmitting fiber with diameter of 1mm and surrounded by 16 receiving fibers with diameter of 0.25mm. The light source is a He-Ne laser with a peak wavelength at 594nm. The light source is externally modulated by a chopper at 200Hz and is used in conjunction with lock-in amplifier to reduce noise resulting from DC drift and interference of ambient stray light. This sensor uses a real reflecting object as target, which is displaced from the bundled fiber end facet using a translation stage. The stage is driven by a piezoelectric motor to provide a fine movement of the real object.

In this experiment, the lock-in amplifier output voltage resulting from the reflected light is recorded automatically by a computer at various displacement distances from the object using Delphi software via serial port RS232. The piezoelectric picometer used in the experiment provides a precise step of 25-30nm for every positive pulse applied. Displacement measurement is carried out with distance steps of 13μm. The surface roughness of the real object is estimated from the displacement curve of the sensor. The light beam leaving the transmitting fiber is reflected back in the form of expanding cone of light towards the receiving fiber, which routes the collected light into silicon photo-detector where its intensity is measured. The intensity of the collected light is a function of lateral movement of the object while the surface of metals is maintained perpendicular to the displacement axis. The experiment is then repeated using three different metal; stainless steel, aluminum and copper.

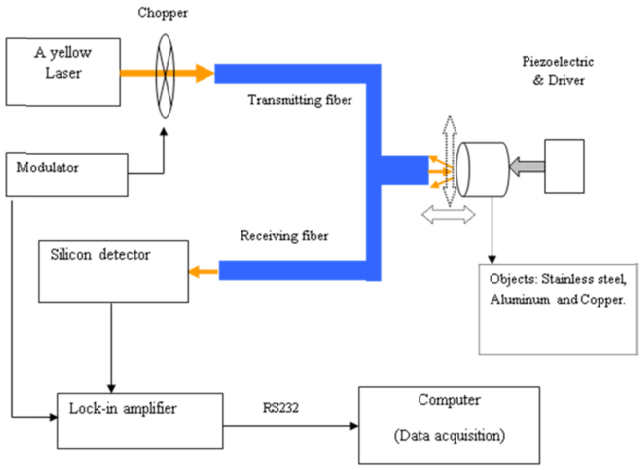

Fig.5.1: Schematic diagram of metal surface roughness based on fiber optic displacement sensor.

Fig. 5.2 shows the characteristic of output voltage of the lock-in amplifier as a function of axial displacement for various metal surfaces (stainless steel, aluminum and copper). The sensor output function (i.e. light intensity versus distance to target flat metal surface) indicates three regions: the blind region, the linear region and nonlinear region. When the gap between the probe tip and the target is very close to zero, light from the transmitting fiber would be reflected back into itself and little or no light would be transferred to the receiving fibers. This is referred to as the blind region. As the distance increases, the reflected cone overlaps with the receiving fibers and hence the output intensity increases. This relation is continued until the entire face of receiving fiber is illuminated with the reflected light. This is the point where maximum voltage is measured and is called optical peak. As the gap increases beyond this transition region, the intensity drops off following roughly an inverse-square law.

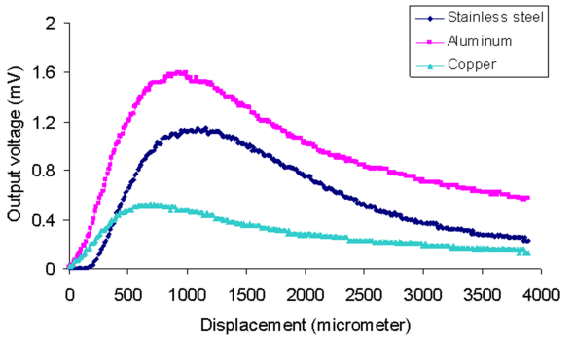

Fig. 5.2: Output voltage against object displacements for various real objects.

The sensitivity of the sensor is determined by the linear portion of the curves. As shown in Fig. 5.2 and discussed in earlier chapters, the sensor has two slopes; front and back slopes, with the front slope showing a higher sensitivity. The linear range, sensitivity, as well as the resolution is summarized in table 5.1for the different reflect targets, and the detailed discussions can be found in section 3.2.1.2.

Table 5.1: The features of the fiber optic displacement (front slope) for various metal surface objects

No.	Type of metal rod and diameter (mm)	A linear range (μm)	Sensitivity (mV/μm)	Resolution (μm)
1.	Aluminum, 10.0mm	520 (104-624)	0.0026	6
2.	Stainless steel, 10.0mm	559 (221-780)	0.0019	7
3.	Copper, 8.0mm	351 (104-455)	0.0011	5

For roughness measurement, the object is fixed within the linear range of the front slope. Then, the output voltages are measured as a function of lateral movement to estimate the roughness of the surface. The fiber tip is held perpendicular to the sample surface. The intensity of the reflected light from the metal surface depends on the

surface texture of the metal and stand-off distance between the surface and fiber tip. Fig. 5.3 (a) shows the output voltage as a function of the position of surface aluminum for 5 lines scanning. As shown in the Fig.5.3 (a), the output voltage has an almost constant value for the whole surface of the metal with a small fluctuation. Fig. 5.3(b) shows 3D views of level roughness of the aluminum surface, which was obtained by 28 lines of scanning on the surface at various lateral position. The 5 lines and 28 lines scanning are means vertical and horizontal detection points. Surface roughness is defined as the difference in detected intensity between the smallest and largest displacements between the fiber tip and the metal surface. The level of roughness is obtained at around 27%, which corresponds to distance variation or maximum gap of about 52μm.

The experiment was then repeated for stainless steel with the results shown in Figs. 5.4 (a) and 5.4 (b). As shown in both Figs, the level of roughness is obtained at around 26%, which corresponds to distance variation or maximum gap of about 37μm. Figs. 5.5 (a) and 5.5 (b) show the results of surface roughness measurements for the copper surface. These results show that the level of roughness is approximately 20% which corresponds to distance variation or maximum gap of about 37μm. Table 5.2 summarizes the experimental results for all metal surface roughness. The surface roughness parameter used throughout in this work is the average surface roughness (R_a) as it is the most widely used parameter by researchers and in the industry as well. It is

the arithmetic average of the absolute value of the height of roughness irregularities from mean value measured, that is:

$$R_a = \left(\sum_{i=1}^{n} |y_i| \right) / n \qquad (5\text{-}1)$$

where y_i is the height of roughness irregularities from mean value and n is the number of sampling data. The value of R_a of the metal surface finish samples as summarized in Table 5.2. The reflectivity of stainless steel, aluminum and copper is obtained at 74%, 70% and 64%, respectively.

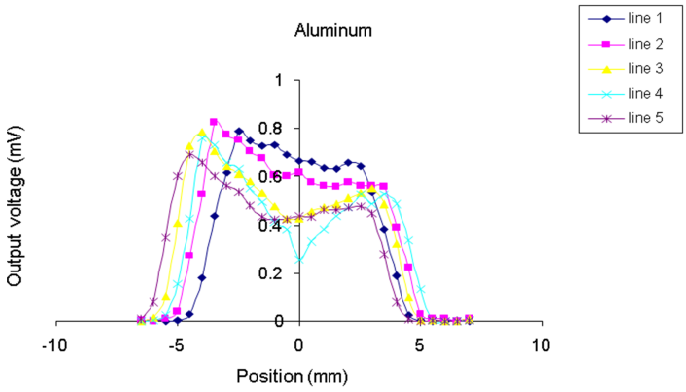

(a) Output voltage against position for scanning at various lines.

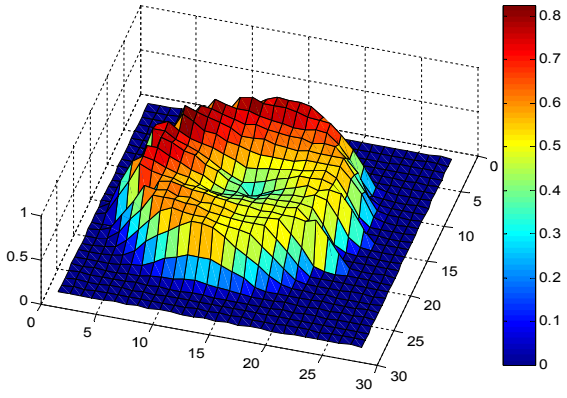

(b) 3D views of a level of roughness of the aluminum surface profile.

Fig. 5.3: Roughness measurement of the aluminum surface profile (a) 2D profile (b) 3D profile.

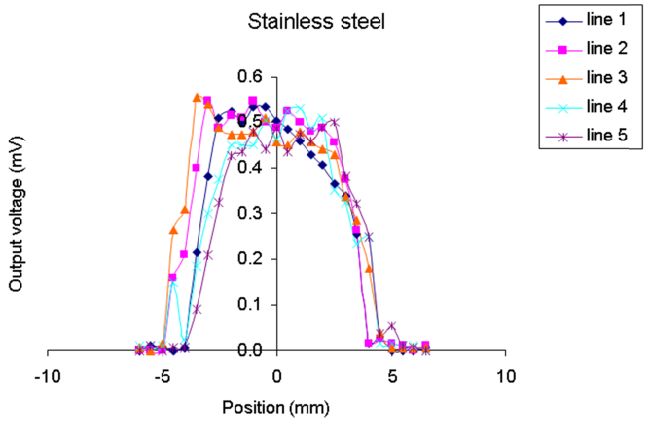

(a) Output voltage against position for scanning at various lines.

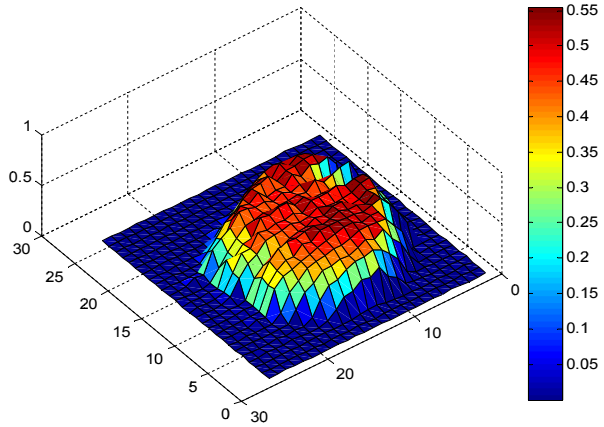

(b) 3D views of a level of roughness of the stainless steel surface profile.

Fig. 5.4: Roughness measurement of the stainless steel surface profile (a) 2D profile (b) 3D profile.

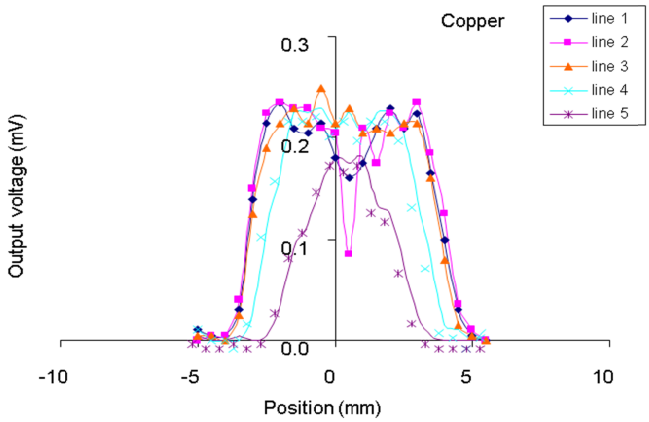

(a) Output voltage against position for scanning at various lines.

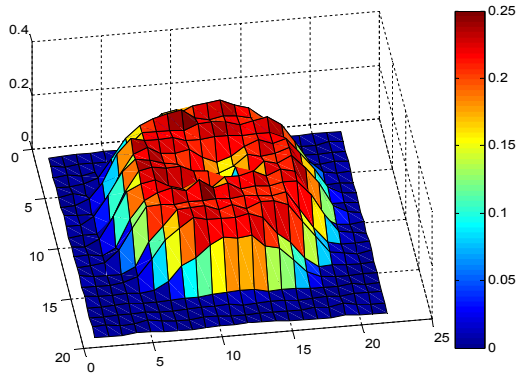

(b) 3D views of a level of roughness of the copper surface profile.

Fig. 5.5: Roughness measurement of the copper surface profile (a) 2D profile (b) 3D profile.

Table 5.2: Level of surface roughness and surface finish parameter (R_a) for various metal surfaces.

No.	Type of metal surface	Level of roughness (%)	Level of roughness (µm)	Average surface roughness, R_a(µm)
1.	Aluminum	8-27	15-52	33
2.	Stainless steel	8-26	19-37	30
3.	Copper	7-20	13-37	22

5.3 Liquid Refractive index Detection Using the FODS

The FODS has a capability to measure physical quantities such as displacement, vibration, strain, pressure, etc [8-10]. However, the use of FODS sensors for detection of environmental refractive index change has not been fully explored. Refractive index sensing is important for biological and chemical applications since a number of substances can be detected through measurement of their refractive index. In the development of a liquid refractive index sensor (LRIS) [11-15], the use of intensity modulation in conjunction with multimode plastic fiber is the most suitable technique due to its non-contact sensing nature and efficient signal coupling.

A FODS based refractive index measurement using a bundled fiber is first introduced by Suhadolnik et al. in 1995 [11]. Later, Chaudhari and Shaligram reported the study of LRIS using various types of optical sources [12]. In our earlier work, FODS based on two asymmetrical fibers for liquid refractive index measurement was proposed [13] as shown in section 3.2.3. In this section, a new LRIS technique is studied and demonstrated by using paired fibers bundled at various inclination angles, and the experiments are carried out by the sensing of the refractive index of isopropyl alcohol, water and methanol, as well as an alternative approach is proposed for sensing of glucose concentration in distilled water based on a FODS, experimentally.

5.3.1 Theoretical analysis and numerical results of proposed LRIS

The structure of the proposed LRIS is shown in Fig. 5.6, which consists of a pair of transmitting and receiving fiber. We assume that the transmitting and receiving fibers have inclination angles of θ_1 and θ_2, respectively against the y-axis. The image of transmitting fiber is located opposite the mirror with the same distance. The center of the receiving fiber and the image of transmitting fiber are marked as O' and O, respectively. From the geometrical analysis of Fig. 5.6, the angle $\alpha = \sin^{-1}(NA/n)$ and $z_a = \frac{r_1}{\tan\alpha}$. Therefore, the following distances are given by,

$$AB = \sqrt{{z_a}^2 + {r_{d1}}^2}\sin\left(\tan^{-1}(\frac{r_{d1}}{z_a}) - \frac{\pi}{2} + \theta_1\right) \tag{5-2}$$

$$O'C = 4r_{d1}\sin\theta_1 + 2x - AB - r_{d2}\sin\theta_2 \tag{5-3}$$

$$OA = \sqrt{{z_a}^2 + {r_{d1}}^2}\cos\left(\tan^{-1}(\frac{r_{d1}}{z_a}) - \frac{\pi}{2} + \theta_1\right) \tag{5-4}$$

$$OC = OA + r_{d2}\cos\theta_2 \tag{5-5}$$

$$OO' = \sqrt{O'C^2 + OC^2} \tag{5-6}$$

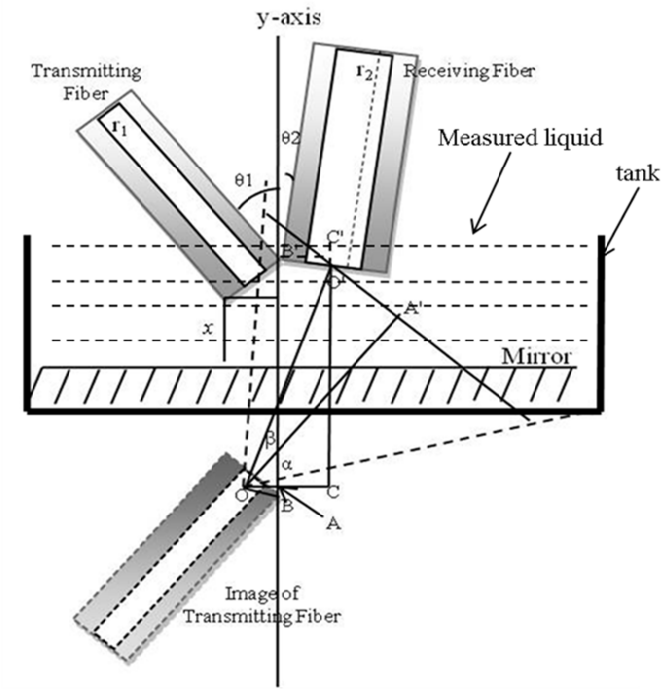

Fig. 5.6: Structure of sensor probe for the sensing of liquid refractive index.

where NA is the numerical aperture of transmitting fiber, n is refractive index of liquid, r_1 and r_2 are the core radius of transmitting fiber and receiving fiber while r_{d1} and r_{d2} are the radius of transmitting fiber and receiving fiber, respectively. x is the displacement between the sensor probe tip and reflector mirror.

Also from the geometrical analysis, the acceptance angle β of the light cone from the virtual point source O, is given by

$$\beta(z) = \tan^{-1}\left(\frac{O'C}{OC}\right) - \frac{\pi}{2} + \theta_1 \qquad (5\text{-}7)$$

The intensity of light emitted from the transmitting fiber can be represented by Gaussian distribution [2] and is given by;

$$I(r,z) = \frac{2P_E}{\pi\omega^2(z)} \exp\left(-\frac{2r^2}{\omega^2(z)}\right) \qquad (5\text{-}8)$$

where*r* is the radial coordinate, *z* is the longitudinal coordinate. $\omega(z)$ is the beam radius expressed as a function of *z*, $\omega(z) = \omega_0\sqrt{1+\left(\frac{z}{z_R}\right)^2}$. The waist radius ω_0 and Rayleigh range z_R are the important parameters in the Gaussian Beam function and the detailed description can be found in ref. (2). Eq. 5-8 shows that the light intensity decays exponentially as it moves away radially from the center of the light circle. The radial coordinate *r* of Eq. 5-8 can be determined by;

$$r = OO'\sin\beta \tag{5-9}$$

The longitudinal coordinate is the distance between the sensor probe tip and the virtual laser source point *O*,

$$z = OO'\cos\beta \tag{5-10}$$

For points situated in the far-field $z >> z_R$, the beam radius of the virtual point source can be derived as [9],

$$\omega(z) \approx z\alpha \tag{5-11}$$

By the approximation,

$$r_1 = z_a \tan\alpha \approx z_a\alpha \tag{5-12}$$

Based on the properties above, the power harnessed by the receiving fiber, *P* can be evaluated by integrating the Gaussian distribution function of Eq. 5-8 over the area of the of receiving fiber end facet S_r,

$$P(r,z) = \int_{S_r} I(r,z)dS_r \tag{5-13}$$

where the core area of the receiving fiber is

$$S_r = \pi r_1^2 = \pi z_a^2 \alpha^2 \tag{5-14}$$

By combining and substituting Eqs. (5-9), (5-10), (5-11) and (5-14) into Eq. (5-13), the proposed LRIS response can be summarized as;

$$P_{(z,r)} = \frac{2P_E}{\pi\omega^2(z)} \exp\left(-\frac{2r^2}{\omega^2(z)}\right) \times S_r = \frac{2z_a{}^2 P_E}{z^2} \exp\left(\frac{2r^2}{z^2\alpha^2}\right) \tag{5-15}$$

This equation shows that the liquid refractive index response of the sensor is a function of displacement x and refractive index n of surrounding medium while the sensor probe is designed with inclination angles of θ_1 and θ_2. Therefore, based on Eq. (5-15), the proposed LRIS can be used to detect liquid refractive index where the sensor probe is immersed in the liquid to be measured.

The mathematical model of the proposed LRIS is simulated using MATLAB program. In the simulation, the wavelength of the laser source λ and numerical aperture NA is set at 594nm and 0.32, respectively. The fiber core radius r_1 and r_2 are set at 0.25mm and 0.5mm while the fiber diameters r_{d1} and r_{d2} are set at 0.5 mm and 0.75mm, respectively.

Simulation results are illustrated in Fig. 5.7. This figure shows the relationship between the sensor response and probe inclination angles $\theta_1$and θ_2 in the measurement of three different refractive indices 1, 1.3 and 1.6 based on probe inclination with same angles of 0, 10˚ and 20˚C. In Fig. 5.7, the output powers are normalized to 1 and the

displacements are simulated in *mm*. Three different group curves are showing three sensor responses based on the three inclination angles set. As seen in Fig. 5.7, it was found that the inclination angles θ_1 and θ_2 affect the displacement curves profile and output power. The highest output power is almost 10 times of the lowest output power. The vertical dash lines are located at displacements of 1.1 mm, 2.0 mm and 3.4 mm corresponding to the sensor probe inclination angles 20˚, 10˚ and 0, respectively. In those positions, the sensor responses have the biggest output difference with the increase of refractive indices from 1.0 to 1.5.The sensor output intensity increases almost linearly with the increase of the refractive index of the probed medium. From Fig. 5.7, we can also observe that the increase of inclination angle improves the performance of the LRIS. The larger the inclination angles of θ_1 and θ_2, the better the performance of liquid refractive index response.

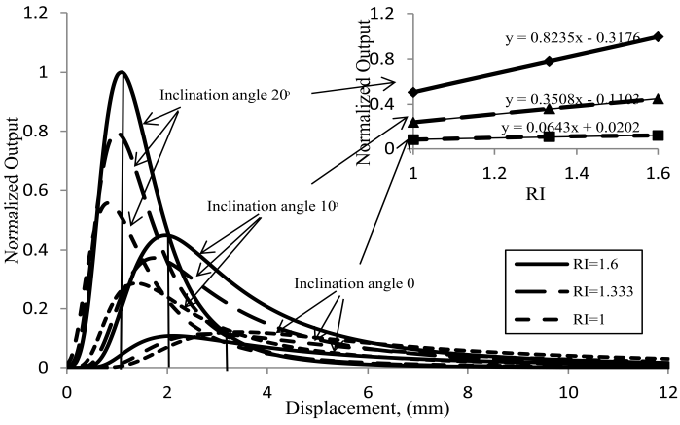

Fig. 5.7: Simulation results for the displacement at various inclination angles and refractive indices. Inset shows the maximum normalized output against the refractive index for inclination angles of 0˚, 10˚ and 20˚(θ_1=θ_2).

Inset of Fig. 5.7 shows the maximum normalized output of the sensor as a function of refractive index for various inclination angles. The normalized outputs were taken at the sensor probe positions of 1.1 mm, 2.0 mm and 3.4 mm for inclination angles of 20˚, 10˚ and 0˚, respectively, which is indicated by vertical dash lines in Fig. 5.78. It was found that the sensitivities of the sensor increases with the increment of probe inclination angle. As shown in the inset of Fig. 5.7, the highest sensitivity of 0.8235 is achieved by the use of probe with inclination angle of 20˚ which is almost 13 times higher than that in zero inclination. Fig. 5.8 shows the simulation curves of the LRIS at various inclination angles for the receiving and transmitting fibers when the refractive index of liquid is set at 1.3. It is clearly seen that the inclination angle of receiving fiber θ_1 has a stronger effect in the sensor output compared to the angle of the transmitting fiber, θ_2. As shown in Fig. 5.8, the highest output power is achieved by the combination of inclination angles $\theta_1 = 20^\circ$ and $\theta_2 = 10^\circ$. The lowest output power is observed when the inclination angles of θ_1 and θ_2 are set at 0˚ and 10˚, respectively. These results show that the sensor sensitivity can be increased by increasing the inclination angle especiallyθ_1. However, increment of the inclination angle is very difficult to be implemented in the experiment unless we can control the position of both fibers to a high degree of precision.

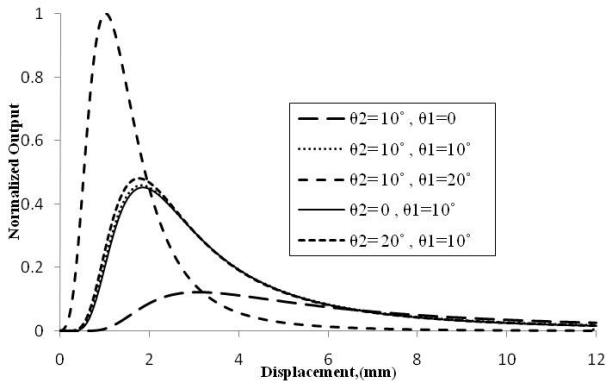

Fig. 5.8: The output power against displacement for various probe inclination angle combinations when the refractive index is set at 1.3.

5.3.2 Experiment setup and measurement results of isopropyl alcohol, water and methanol

Fig. 5.9 shows the experimental set-up, which consists of a 594nm yellow He-Ne laser as a light source and a bundled fiber as probe. The emitted laser light has an average output power of 3.0mW, beam diameter of 0.75mm and beam divergence of 0.92 mRads. The external chopper modulates the light at a frequency of 200 Hz before it is coupled into the transmitting fiber. The transmitting fiber transfers the modulated light from the laser source to the reflector mirror while the receiving fiber collects the reflected light and channels it to the detector. The sensor probe is mounted on the stage controlled by NewFocus Picomotor for the displacement measurement. Silicon detector measures the received light and converts it into electrical signal which is then analyzed using the lock-in amplifier. During the measurement, the room temperature is kept at 28 ºC to avoid the change of liquid refractive index with temperature.

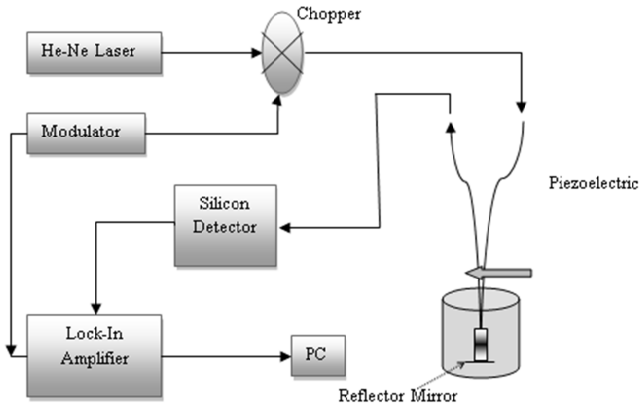

Fig. 5.9: Experimental set-up of the proposed liquid refractive index sensor

In our experiment, three different liquids: isopropyl alcohol, water and methanol are used as the surrounding medium. Two inclination angles for both transmitting and receiving fibers are used, which are 0˚ and 10˚ for both fibers. The refractive index of isopropyl alcohol, water and methanol are 1.377, 1.333 and 1.329, respectively. The sensor performance with air as surrounding medium is also carried out for comparison purpose. During the experiment, the sensor probe is mounted onto the stage and the liquid tank is fixed on the experiment table. The liquid in the tank is changed without moving the tank to ensure the consistency of the measurement. The room temperature was kept at 28° to ensure that the refractive index of the liquid is maintained. Only the displacement parameter is changed in the experiment.

Fig. 5.10 shows the displacement curve at various surrounding media when the inclination angles are set at 0° for both transmitting and receiving fibers. As shown in this figure, the normalized peak output power increases from 0.83 to 1.00 as the refractive index increases from 1.329 (methanol) to 1.377 (alcohol). It is also found that

the displacement position for the peak output increases from 4.0 to 5.1 mm as the refractive index increases from 1.329 to 1.377. This is attributed to the change of acceptance cone angle that increases with refractive index increase. The larger acceptance angle provides a mean to collect more signal power. Fig. 5.11 shows the displacement curves when the inclination angles for both fibers are increased to 10°. As seen in Fig. 5.11, the peak power and its position increase with refractive index. The peak position of the curve also increases from 3.0 mm to 3.4 mm as the refractive index changes from 1.329 to 1.377. From these experimental results, it was found that the sensitivity of the sensor with 10°of probe fibers inclination shows a higher sensitivity compared to setup with 0° of probe fibers inclination. The sensitivities obtained are 0.11/mm and 0.04/mm for the sensors setup with 10° and 0° inclination angles respectively. This finding may be useful for chemical, pharmaceutical, biomedical and process control sensing applications.

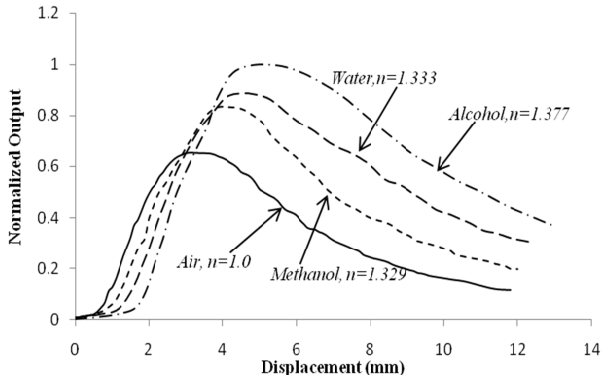

Fig. 5.10: Experiment results of the displacement curve at various liquid materials when the probe inclination angles are set at 0˚ ($\theta_1=\theta_2$).

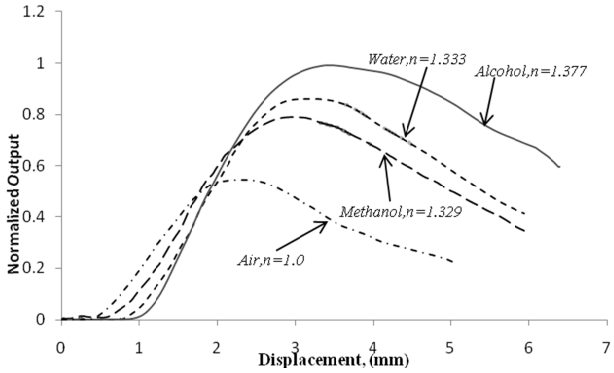

Fig. 5.11: Experiment results of the displacement curve at various liquid materials when the probe inclination angles for both transmitting and receiving fibers are set at $10^{\circ}(\theta_1=\theta_2)$.

5.3.3 Experiment setup and results of detection of glucose concentrations

The schematic experimental set-up for sensing the variation of concentration of glucose liquid solutions is shown in Fig. 5.12. The set-up consists of a yellow He-Ne laser, fiber optic probe or bundled fiber, reflective flat mirror, photodiode, lock-in amplifier and a computer. The fiber optic probe consists of a 2m long PMMA (polymethyl methacrylate) fiber bundle with one transmitting fiber of 1 mm diameter and 16 receiving fibers of 0.25 mm in diameter. Each fiber has a core and cladding refractive index of 1.492 and 1.402, respectively. The light from a He-Ne laser (λ=594nm) is coupled into a transmitting fiber and is emitted at the end of the bundled fiber onto the flat mirror. The reflected light is then collected by the receiving fiber and transmitted to the photodiode. The laser provides an average output power 3.0mW, beam diameter 0.75mm and beam divergence 0.92 mRads. The photodiode is a high

speed photodiode detector housed in a “connector-less” style plastic fiber optic package. Optical response of silicon detector extends from 400 to 1100 nm.

The displacement of the fiber optic probe is achieved by mounting it on a piezoelectric-meter, which is rigidly attached to a vibration free table. The fiber optic probe is immersed into the measuring liquid (solutions of glucose in distilled water). Light from the He-Ne laser (peak wavelength at 594 nm) is coupled into the transmitting fiber. The probe rise vertically from the initial zero point, where the reflective surface and the probe are in close contact. The light source is modulated externally by a chopper with a frequency of 200 Hz and is used in conjunction with lock-in amplifier to reduce DC drift and the interference of ambient stray light. Signal from the detector is converted to voltage and is measured using a lock-in amplifier. The fiber optic probe is first immersed in distilled water; the output intensity is measured by changing the position of the fiber optic probe from 0 to 10 mm in steps of 50 μm. The measurements are then carried out for glucose solutions (Merck KGaA Darmstadt, Germany) with concentrations of 2.5, 5.0, 7.5, 10 and 12.5 g per 50 ml of distilled water. During the experiment, error due to temperature variation is negligible as the temperature is kept constant at 25°C.

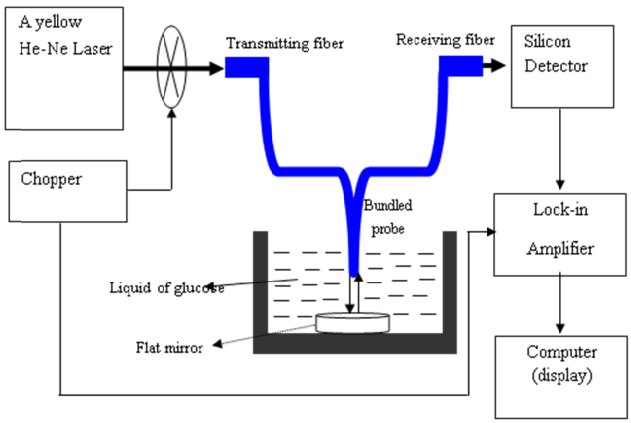

Fig. 5.12: Schematic experimental setup for sensing the variation of glucose concentration.

Fig. 5.13 shows the reflected light intensity versus distance of the reflecting target from the fiber optic probe at various glucose concentrations. In the experiment, the glucose concentration is varied from 0 to 12.5 g per 50 ml of distilled water. The displacement curves exhibit a maximum with a steep front slope while the back slope follows an almost inverse square law relationship. The signal is zero at small distances, because the light cone does not reach the receiving fibers. When the displacement is increased, the size of the reflected cone of light at the plane of the fibers end facet increases and start to overlap with the core of the receiving fibers, leading to a small detected output. Further increase in the displacement leads to large overlapping resulting in rapid increase in the output until a maximum is reached. After the maximum point, the output starts to decrease with increasing displacement due to large increase in the size of the light cone, resulting in the decrease of power density. The shift in the peak of the curve in Fig. 5.13 denotes enhanced mode coupling of the receiving fiber

with respect to the increase in glucose concentration. It is seen that when the concentration increases, the peak voltage value also increases and moves towards the left. The variation or of the received light intensity profile is due to the change of immersion concentration, which actually changes the emitting and acceptable angles of the two fibers. The performance of the sensor is summarized in Table 5.3.Front and back slopes sensitivity and linear range are observed to be random for different glucose concentration.

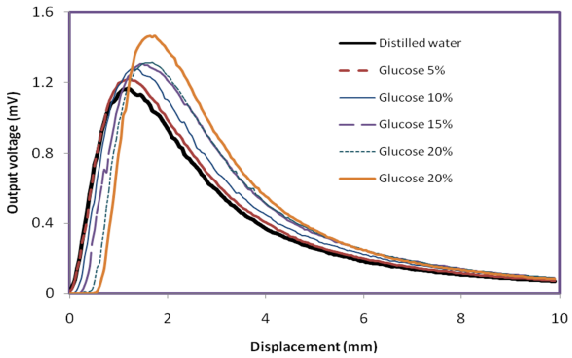

Fig. 5.13: The output voltage as function of the displacement at various glucose concentrations in distilled water.

Fig. 5.14 shows the variation of peak voltage and its position with increasing concentration of glucose. In the present investigation, it is found that the peak voltage increases linearly with glucose concentration at a rate of 0.0103mV/(%), this is for the case when the glucose concentration is varied from 0 to 25%. The peak voltage position also increases linearly with concentration as shown in Fig. 5.14. From the experimental results it can be concluded that the refractive index of glucose solution increases linearly with glucose concentration. This in turn increases the signals received in the

receiving fiber due to the reduced acceptance cone angle. The glucose concentration fiber optic sensor has a measured error of less than 0.6% and the results are repeatable using the current setup. This finding may be quite useful for chemical, pharmaceutical, biomedical and process control sensing applications.

Table 5.3: The performance of proposed glucose sensor

Glucose (%)	Position of peak voltage (mm)	Peak voltage (mV)	Front slope		Back slope	
			Sensitivity (mV/mm)	Linear range (mm)	Sensitivity (mV/mm)	Linear range (mm)
0	1.20	1.167	1.57	0.60 (0.1-0.7)	0,34	2.1 (1.5-3.6)
5	1.20	1.223	1.53	0.7 (0.1-0.8)	0.35	2.15 (1.45-3.6)
10	1.30	1.283	1.60	0.7 (0.2-0.9)	0.34	2.2 (1.8-4.0)
15	1.45	1.305	1.46	0.8 (0.3-1.3)	0.35	2.2 (2.1-4.3)
20	1.65	1.315	1.65	0.75 (0.5-1.25)	0.35	2.45 (1.90-4.35)
25	1.70	1.467	1.86	0.8 (0.6-1.4)	0.42	2.1 (2.1-4.2)

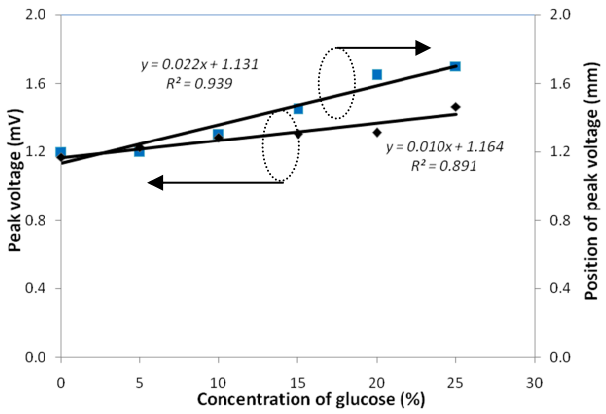

Fig. 5.14: Variations of peak voltage and its position with increased concentration of glucose in distilled water.

5.4 The Monitoring of Liquid Level Using A FODS

Liquid level measurement is important in many areas such as fuel storage system, chemical processing, etc. Liquid level can be detected by mechanical, electrical and optical methods [16-18]. Electrical liquid-level sensors (LLS) are widely employed, but they might not be suitable if the liquid to be measured is conductive, potentially explosive or erosive. Fiber-based LLSs offer many advantages under these challenging conditions since the fiber-optic sensors are non-conducting, anti-erosion and immune to electromagnetic interference. Recently, various approaches have been reported on fiber-optic LLS such as using a fiber Bragg grating (FBG) with bending cantilever beam [19] as well as a technique based on the bending of a multimode fiber [20]. In both methods, the sensing elements need to be submerged inside the liquid to operate. However, the applicability of these immersed sensing elements might be limited in applications involving harsh environments and acidic solutions.

In this section, a simple, cost effective and non-contact intensity based LLS is demonstrated. In the proposed LLS, the sensing probe is linked to a float which is in contact with the measured liquid. This sensor is a type of fiber-optic displacement sensors (FODSs), which simply transforms the sensing of position into the measurement of displacement. The performance of the sensor using two different reflectors is investigated.

The sensing principle and sensor setup

The basic principle of the sensor is the measurement of vertical float displacement resulting from liquid level change. Fig. 5.15 shows a schematic setup of the proposed fiber optic LLS. The setup consists of a water tank, a properly designed float and a concave mirror based FODS. The FODS uses a He-Ne laser operating at wavelength of 594 nm with an average output power of 3.0 mW. The laser beam diameter is 0.75 mm while beam divergence is 0.92 mRads. The light is modulated at a frequency of 200 Hz by an external chopper before being launched into the transmitting fiber. A concave mirror (or flat mirror), located at the end of the transmitting fiber, reflects the guided light from the transmitting fiber into a receiving fiber which is bundled together with the transmitting fiber. Meanwhile, both fibers are attached to an L shape cantilever beam which is connected to a float inside the tank. The receiving fiber guides the light into the photo detector which converts the light power into voltage. A model SR-510 lock-in amplifier is connected to the chopper and photo detector. It functions as a data-acquisition system, matching the phase between the modulated light and chopper and removes the noise generated by laser source, photo detector and amplifier [21].

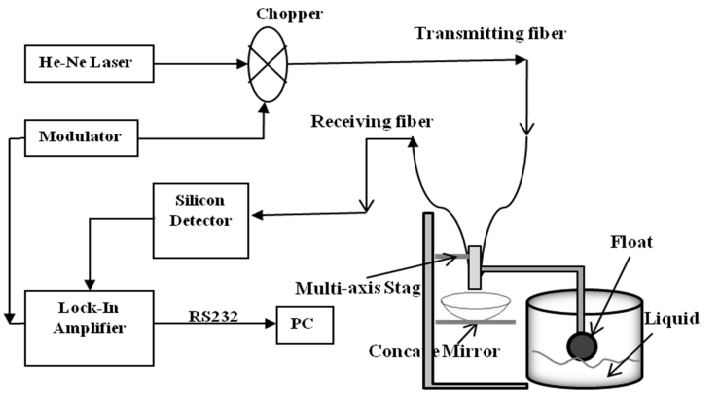

Fig. 5.15: Experimental setup of the proposed liquid level sensor

With a concave mirror as reflector, the characteristic of the proposed sensor, other relevant details and the transfer function of the proposed sensor can be found in section 4.2.1,

$$P(u)=\frac{2z_a^2P_E\left\{1-\exp\left(-\frac{D^2}{2(u+z_a)^2\theta^2}\right)\right\}}{\left[u-\frac{(u+z_a)f}{u-f+z_a}\right]^2\left(\frac{u+z_a}{f}-1\right)^2}\exp\left(-\frac{8z_a^2}{\left[u-\frac{(u+z_a)f}{u-f+z_a}\right]^2\left(\frac{u+z_a}{f}-1\right)^2}\right) \quad (5\text{-}16)$$

where P_E is the emitting power of laser source, u is the distance between the sensor probe tip and concave mirror, $\theta = \sin^{-1}(NA)$ and NA is the numerical aperture of the transmitting fiber. With a flat mirror as the reflector, the transfer function of proposed sensor has been previously analyzed in [23] and is given by

$$P(z)=\frac{2(k+1)^2}{\xi^2}\exp\left(1-\frac{2(1+k)^2}{\xi^2}\right) \quad (5\text{-}17)$$

where k is the ratio of the transmitting fiber core radius to the receiving fiber core radius and ξ is the normalized distance or displacement between the probe and mirror.

From the transfer functions of Eqs. (5-16) and (5-17), it can be seen that the sensor response is only influenced by the focal length f and the diameter of the circular

concave mirror *D* for setup with concave mirror as reflector and by the core radial ratio *k* for setup using flat mirror. As such, the proposed LLS is widely compatible with the various type of FODSs while circumventing the design trade-off in the selection of sensitivity and measurement range which is a typical constraint for conventional fiber optic LLS. Furthermore, no other parameters affect the sensor response except those specified in Eqs.(5-16) and (5-17). Hence, the proposed LLS is insensitive to the surrounding environments.

Results and discussions

Fig. 5.16 depicts the experimental result when the liquid level is moving upward. In this experiment, a concave mirror with a focal length of 10 mm and a diameter of 24 mm is used as reflector. The sensor output intensity is modulated by the rise of the liquid level and the response has six linear slopes of which four of them are located within the vicinity of twice the distance of the focal length (20 mm). This property enables flexible sensing based on the liquid level range of interest by properly choosing the desired focal length. The maximum measurement range of about 25 mm is obtained using a mirror with focal length of 10 mm. The performance of this sensor at various monitoring points or slopes is summarized in Table 5.4. The maximum sensitivity of 1.3015 mV/mm is obtained in a liquid level range of 20.1 mm to 20.9 mm.

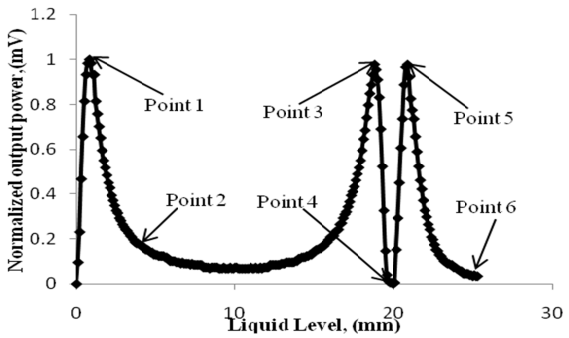

Fig. 5.16: The experimental result of the proposed LLS using a concave mirror as reflector.

The second experiment is carried out using a flat mirror as reflector instead of concave mirror. In this experiment, two different fiber-probes are used; two symmetrical (k=1) and asymmetrical (k=0.5) fibers bundled together. The experimental results are compared in Fig. 5.17, in which two slopes are obtained. As seen in the figure, linear measurement range up to 3 mm and 3.5 mm are observed with k=1 and k=0.5, respectively. The experimental results are summarized in Table 5.4. Fig. 5.17 also illustrates that higher sensitivity is obtained from the curve of k=1 while longer measurement range is achieved by the curve of k=0.5. The output response curve of Fig. 5.17 is observed to be shifted to a longer range as the value of k decreases. Therefore, the sensitivities of the front and back slopes decrease with the lower value of k as shown in Table 5.4. On the other hand, the linear range of the slope is larger with a lower value of k.

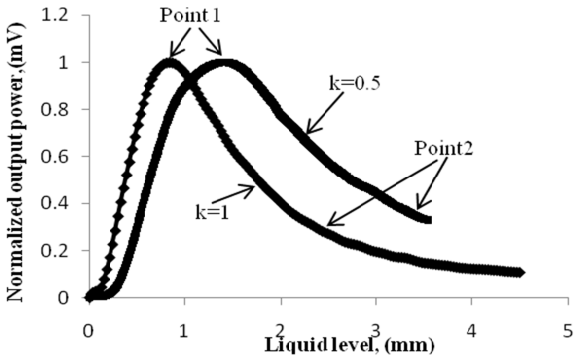

Fig.5.17: The experimental result of the proposed LLS with a flat mirror for two different value of k.

Table 5.4 summarizes the performance of LLS for the three experiments. The highest sensitivity of 1.4533 mV/mm is obtained with a measurement range of 0.84 mm. The largest measurement range of 4.8 mm is obtained from monitoring point 3 when concave mirror is used as reflector. With a flat mirror as a reflector, the sensitivity for k=0.5 decreased by 52.5% and 14.8% for the front and back slope, respectively, when compared to those of k=1. However, the measurement range of front and back slopes increased by 46.2% and 18.8% when compared to those of the k=1. From the analysis, it can be seen that by using various combinations of fiber core diameters and reflector type, ten different sensitivities and linear sensing ranges can be selected according to the requirement of a specific liquid level measurement. In summary, the proposed fiber optic LLS shows good compatibility with other type of displacement sensors while avoiding the trade-off between sensitivity and measurement range which is normally a compromise encountered in the design of conventional fiber optic LLS.

Table 5.4: The sensitivities and measurement ranges of proposed LLS

Methods	Monitoring point	Sensitivity (mV/mm)	Measurement range (mm)
Concave mirror k=1	Point 1	1.4026	0-0.8
	Point 2	0.2649	0.8-3.8
	Point 3	0.1625	14-18.8
	Point 4	1.030	18.9-20
	Point 5	1.3015	20.1-20.9
	Point 6	0.1821	21-25
Flat mirror k=0.5	Point 1	0.9529	0.1-1.4
	Point 2	0.3443	1.4-3.5
Flat mirror k=1	Point 1	1.4533	0-0.84
	Point 2	0.3951	0.84-3

5.5 Vibration measurement

Vibration sensors are useful for monitoring the condition of rotating machinery, as overheating or excessive vibration indicates excessive loading, inadequate lubrication, or bearing wear [24]. Traditional magneto-electric vibration sensors and servo accelerometer have severe shortcomings when used to measure vibration where low frequency components predominate. Mechanical and electrical vibration sensors require physical contact during measurement. On the other hand optical sensor is used to measure low frequency vibration and does not require any physical contact and do not perturb the source of vibration [25].Fiber-optic vibration sensor can be classified into

three categories according to their working principle; wavelength, phase and intensity modulation based sensors. The first type is based on the measurement of wavelength changes due to vibration signals. This technique normally requires specially designed mechanical devices (transducers) to enhance its sensitivity. The second type uses an interferometer such as Michelson or Mach-Zehnder [26] to interrogate the phase shift of the sensor caused by vibration and has very high sensitivity but they exhibit low stability and impose stringent mechanical requirements because the alignment is critical. These approaches are characterized by excellent performances but require complex and expensive setups and are not economical for mapping of vibration amplitude at several test points. The third type takes the advantage of change in intensity with vibration. This intensity modulated extrinsic sensor normally used a plastic optical fiber (POF) as probe and therefore provides many advantages such as small size, light weight, geometrical versatility, EMI immunity and ease of multiplexing and de-multiplexing [27].

In this section, a rugged, low cost and very efficient FODS is proposed for the measurement of amplitude and frequency of vibration of load speaker using the third approach. The schematic representation of the experimental set-up for fiber optic vibration sensor is shown in Fig. 5.18. The sensor device consists of a fiber optic transmitter, bundled POF probe, load speaker, audio amplifier and a silicon detector. The fiber optic probe consists of two POFs of length 2m, which consists of one transmitting fiber with diameter of 1.0mm and 16 receiving fibers with diameter of 0.25

mm. All fibers have a numerical aperture of 0.5. The bending losses are minimized by placing both fibers in close contact, thus forming an equal radius of curvature.

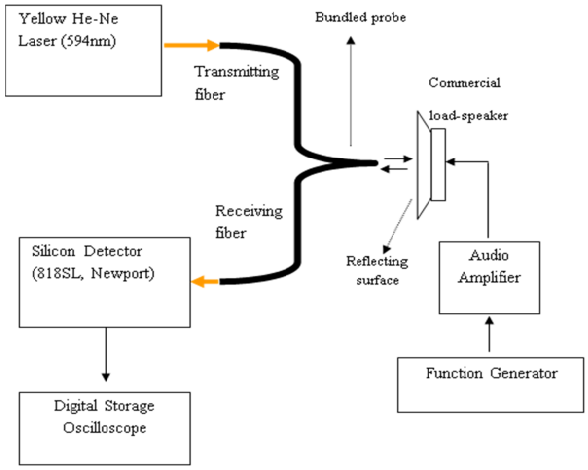

Fig. 5.18: Schematic diagram of the vibration sensor using fiber optic displacement sensor.

A reflective surface is pasted on a load speaker and the probe is held in position perpendicular to the reflective surface. The static displacement of the fiber optic probe is achieved by mounting it on a piezoelectric displacement meter, which is rigidly attached to a vibration free table. Yellow light from He-Ne laser at peak wavelength of 594nm is coupled into the transmitting fiber. The initial position of the probe is at zero point, where the reflective surface and the probe are in close contact. In this case, the probe is placed in a way such that the detector output corresponds to the center of the linear slope region of its characteristic curve. The signal from the detector is converted to voltage and is measured by a digital multimeter. The investigation consists of recording the output voltage from the detector at probe distances ranging from 0 to 6 mm in steps of 12 μm. The experiments are repeated for different frequencies of

vibration ranging from 200 to 350 Hz and the vibration amplitudes are measured for different driving voltages.

Fig. 5.19 shows the variation of output voltage with different displacement of fiber optic probe from the reflecting target. As shown in the figure, the curve exhibits a maximum with a steep front slope and back slope which follows an almost inverse square law relationship. The maximum sensor output voltage obtained is 1.65mV for a distance of 1.2mm between the reflective surface and the fiber optic probe. The sensitivity of the sensor on either side can be obtained from the slope of the curve. Thus a sensitivity of 0.0029mV/μm is obtained within a range from 325 to 650μm for the front slope and a sensitivity of 0.0005mV/μm can be achieved over a range from 1300 to 3500μm for the back slope.

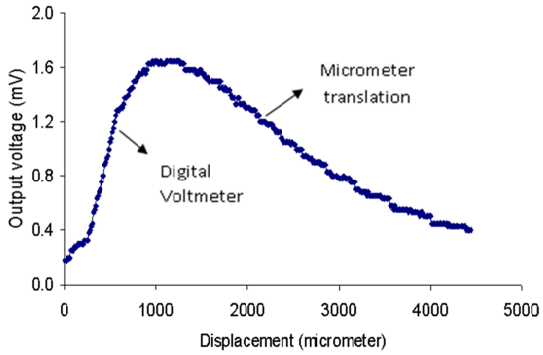

Fig. 5.19: Variation of the output voltage with the axial displacement of the load speaker from bundled probe.

Fig. 5.20 shows the vibration amplitude against driving voltage at different frequency of vibration. The sensor is capable of measuring vibration amplitude ranging from 0.22 mm to 0.44 mm within a frequency range of 200 to 350 Hz. As shown in Fig.

5.20, the variation of the vibration amplitude with driving voltage is higher at lower frequencies of vibration. Fig. 5.21 compares input and output signal of the vibration fiber optic sensor at 250 Hz. The input signal is detected after the audio amplifier while the output signal comes out from the receiving fiber. Both waveforms have the same frequency of 250Hz with the output signal showing a higher noise.

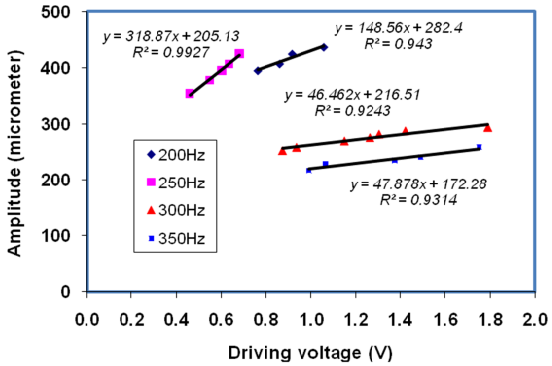

Fig. 5.20: Output voltage as function of driving voltage of the fiber optic vibration sensor.

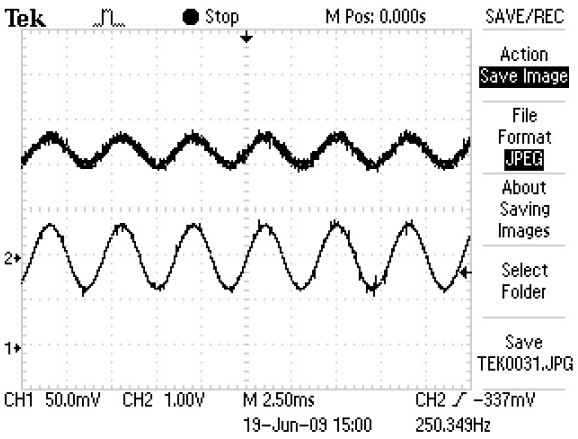

Fig. 5.21: Original input signal (lower) and the measured output signal (upper) of the vibration sensor.

Figs. 5.22(a) and (b) represent the fast Fourier transform (FFT) spectra for mechanical vibrations corresponding to 300 Hz and 350 Hz, respectively. The FFT

spectral response clearly shows that output from the vibration sensor can be resolved into corresponding characteristic frequencies of the measured vibration. The spectra also show higher harmonics. Possible sources of error in current sensor operation are light source fluctuation, stray light and possible mechanical vibrations. To reduce these effects a well-regulated power supply is used for the yellow He-Ne laser and this minimizes the fluctuation of source intensity. The sensor fixture is also designed so that stray light cannot interfere with the source light. To reduce mechanical vibrations, the experimental set-up is arranged on a vibration free table. The simplicity of the design, high degree of sensitivity, dynamic range and low cost of fabrication make it suitable for field applications.

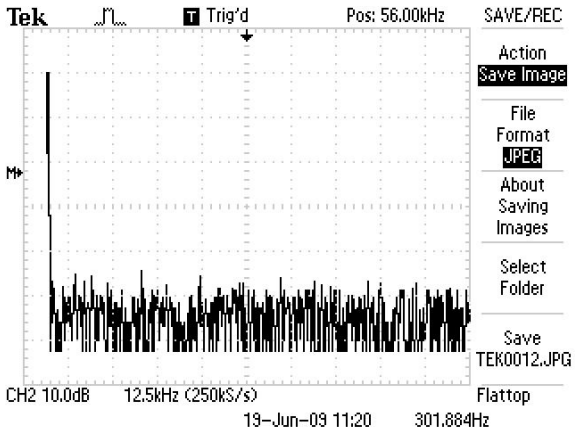

(a)

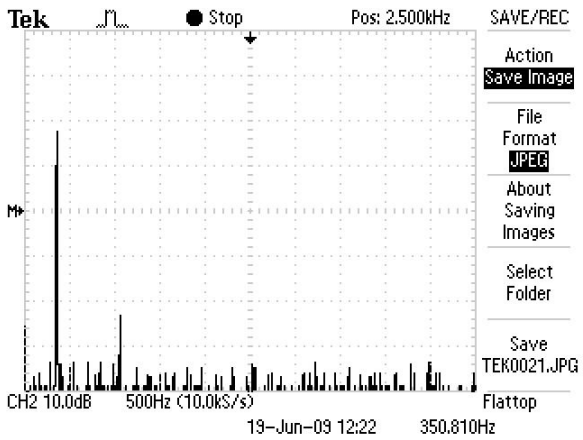

(b)

Fig. 5.22: FFT signal from fiber optic vibration sensor (a) 300Hz and (b) 350Hz.

5.6 Summary

Four applications of FODS are reviewed in this chapter. In these applications, the estimation of surface roughness of metals is first discussed. It is based on intensity modulation technique and uses a multimode plastic bundled fiber as probe and He-Ne laser as light source. The surface roughness of three types of metals is investigated by fixing the object within the linear range of the front slope and measuring the output voltage as a function of lateral displacement. The level of roughness for aluminum, stainless steel and copper samples are estimated to be approximately 27%, 26% and 20% respectively.

In the following section, a simple liquid refractive index sensor is theoretically and experimentally demonstrated using FODS with a pair of bundled fiber which is angled to increase the sensitivity, and a detection concentration of glucose also

demonstrated based on a FODS with a concentric type of sensor probe. Through the theoretical analysis, a highest sensitivity of 0.8235 is achieved with the probe inclined at 20˚ which is almost 13 times higher than that with 0˚ inclinations. Both theoretical and experimental results show that the peak power and the location of the displacement curve changes with refractive index. It was also found that the sensitivity of the sensor with 10° inclination shows a higher sensitivity compared when a straight probe is used. The sensitivities are obtained at 0.11/mm and 0.04/mm for sensors with 10° and 0° inclination angles respectively. In the experimental of detection glucose concentration in distilled water, the experimental results show that the peak voltage or light intensity and its position increase linearly with the glucose concentration. The sensitivity is measured to be around 0.0103mV/(%) when the glucose concentration is varied from 0 to 25%.

An extra-low cost, ultra-high sensitivity, and widely compatible fiber optic LLS is proposed and demonstrated in the next section. A float which is in contact with the liquid surface converts the position of the liquid level to the distance between of the fiber probe and the reflector. This is done via an L-cantilever beam which is fixed to the sensor probe. The response of the sensor probe is influenced by the distance between the probe and the reflector. The sensor probe is not in contact with the measured liquid. Three various experiments are conducted to prove the proposed sensor has very wide compatibility with other type of FODSs. With a concave mirror, six

measurement slopes within a range of 25 mm are observed with the maximum sensitivity of 1.3015mV/mm. With a flat-mirror two measurement slopes are observed with the highest sensitivity of 1.4533mV/mm and the longest measurement range of 4.8mm. A flexible selection of sensitivity and measurement range is achieved by proposed sensor from free choose of FODSs.

In the fourth section, an extrinsic bundled POF displacement sensor has been proposed for the measurement of amplitude and frequency of vibration. The displacement curve exhibits the maximum output voltage of 1.65mV at a distance of 1.2mm between the reflective surface of the speaker and the fiber optic probe. The sensor is capable of measuring vibration amplitude ranging from 0.22 mm to 0.44 mm within a frequency range of 200 to 350 Hz. The sensitivity of the sensor is found to be 0.0029mV/μm over 325 to 650μm range and -0.0005mV/μm over 1300μm to 3500μm range.

References

[1]. M. L. Bechwith, “Mechanical measurement”, Addison Wesley Longman, (2000).

[2]. J. Chang, Q. Wang, X. Zhang, L. Ma, T. Liu, Q. Wang, Z. Liu, S. Zhang and S. Ding, "Single-end vibration sensor based on an over-coupled fiber-loop reflector,” Laser Physics, Vol. 18, pp. 452-454, (2008).

[3]. H. Arellano-Sotelo, Yu. O. Barmenkov and A.V. Kir'yanov**, "**The use of erbium fiber laser relaxation frequency for sensing refractive index and solute concentration of aqueous solutions,**"** Laser Physics Letters, Vol. 5, No. 11, pp. 825-829, (2008).

[4]. P. M. Sandeep, S. W. B. Rajeev, M. Sheeba, S. G. Bhat, V. P. N. Nampoori**,** **"**Laser induced fluorescence based optical fiber probe for analyzing bacteria,"Laser Physics Letters, Vol. 4, No. 8, pp. 611-615, (2007).

[5]. I. P. Radko, V.S. Volkov, S.I. Bozhevolnyi, J. Henningsen, J. Pedersen, **"**Near-field mapping of surface refractive-index distributions,"Laser Physics Letters, Vol. 2, No. 9, pp. 440-444, (2005).

[6]. U. Person, "A fiber-optic surface-roughness sensor," Journal of Materials Processing Technology, vol. 95, pp. 107-111, (1999).

[7]. A. B. Ganesh, T.K. Radhakrishnan, G. Gobi, D. Sastikumar, "Estimation of Corrosion of Metals Using Fiber Optic Displacement Sensor System," Sensors & Transducers Journal, vol.70, pp.645-654, (2006).

[8]. M. Yasin, S.W. Harun, H.A. Abdul-Rashid, Kusminarto, Karyono, H. Ahmad, **"**The performance of a fiber optic displacement sensor for different types of probes and targets," Laser Physics Letters, Vol. 5, No. 1, pp. 55-58, (2008).

[9]. M. Yasin, S. W. Harun, Samian, Kusminarto and H. Ahmad, “Simple design of optical fiber displacement sensor using a multimode fiber coupler,” Laser Physics, Vol. 19, No.7, pp. 1446-1449, (2009).

[10]. P. K. Rastogi, “Optical Measurement Techniques and Applications”, Artech House, Inc.Boston, London, (1997).

[11]. A. Suhadolnik, A. Babnik, J. Mo2ina,“Optical fiber reflection refractometer”, Sensor and Actuators B, Vol. 29, pp.428- 432, (1995).

[12]. A.L. Chaudhari and A.D. Shaligram, “Multi-wavelength optical fiber liquid refracto-metry based on intensity modulation”, Sensor and Actuators A, Vol.100, pp.160- 164, (2002).

[13]. H. Z. Yang, S. W. Harun and H. Ahmad, “Fiber Optic Displacement and Liquid Refractive Index Sensors with Two Asymmetrical Inclined Fibers”, Sensor and Transducer, Vol.108, pp. 80-88, (2009).

[14]. P. Nath, H.K. Singh, P. Datta, K.C. Sarma, “All-fiber optic sensor for measurement of liquid refractive index”, Sensor and Actuators A, Vol.148, pp.16-18, (2008).

[15]. V. Kleiza1 and J. Verkelis, “Some Advanced Fiber-Optic Amplitude Modulated Reflection Displacement and Refractive Index Sensors”, Nonlinear Analysis: Modelling and Control, Vol. 12, No. 2, pp. 213–225, (2007).

[16]. K. Shannon, X. Li, Z. Wang, J. D. N. Cheeke, “Mode conversion and the path of acoustic in a partially water-filled aluminum tube,” Ultrasonics, Vol. 37 (3) pp. 303–307 (1999).

[17]. N. B. Manik, S. C. Mukherjee, A. N. Basu, “Studies on the propagation of light from a light-emitting diode through a glass tube and development of an optosensor for the continuous detection of liquid level,” Opt. Eng., Vol. 40 (12), pp. 2830–2836, (2001).

[18]. B. F. Yun, N. Chen, and Y. P. Cui, “Highly sensitive liquid level sensor based on etched fiber bragg grating,” IEEE Photonic Technology Letters, 19, 1747-1749, (2007).

[19]. K. R. Sohn, and J. H. Shim, “Liquid level monitoring sensor system using fiber bragg grating embedded in cantilever,” Sensors and Actuators, A, 152, 248-251, (2009).

[20]. X. W. Dong, and R. F. Zhao, “Detection of liquid level variation using a side polished fiber bragg grating,” Optics & laser technology, 42, 214-218, (2010).

[21]. M. Lomer, J. Arrue, C. Jauregui, P. Aiestaran, J. Zubia, and J. M. Lopez-Higuera, “Lateral polishing of bends in plastic optical fibers applied to a multipoint liquid level measurement sensor,” Sensors and Actuators A, 137, 68-73, (2007).

[22]. H. Z. Yang, K. S. Lim, S. W. Harun, K. Dimyati, and H. Ahmad, “Enhanced Bundle Fiber Displacement Sensor Based on Concave mirror” Sensors and Actuators A, 162, 8-12, (2010).

[23]. K. S. Lim, S. W. Harun, H. Z. Yang, K. Dimyati, H. Ahmad, “Analytical and experimental studies on asymmetric bundle fiber displacement sensors”, J. of Modern Optics, Vol. 56, pp.1838-1842, (2009).

[24]. Girao P.M. B. S., Postolache O.A., Faria J., Pereira J. M. C. D., "An overview and a contribution to the optical measurement of linear displacement", IEEE Sensors Journal, vol. 1, no. 4, (2001) 322-331.

[25]. Guiju Song, Xiangzhao Wang, Zujie Fang, “White-light interferometer with high sensitivity and resolution using multi-mode fibers”, Optics, Vol. 112, Issue 6, (2001) 245-249.

[26]. Castellini P., Martarelli M., Tomasini E. P., "Laser Doppler Vibrometry:Development of advanced solutions answering to technology's needs",Mechanical System and Signal Processing, vol. 20, 1265-1285, (2006).

[27]. S. Binu, “Calibration of accelerometers by using an extrinsic fiber optic probe,” Microwave and Optical Technology Letters. Vol. 49, pp. 2700-1703, (2007).